Neuromorphic Vision Hybrid RRAM-CMOS Architecture

Jason Kamran Eshraghian, Jr., *Student Member, IEEE*, Kyoungrok Cho, *Member, IEEE*, Ciyan Zheng, *Student Member, IEEE*, Minho Nam, *Student Member, IEEE*, Herbert Ho-Ching Iu, *Senior Member, IEEE*, Wen Lei, and Kamran Eshraghian

***Abstract*— The development of a bioinspired image sensor, which can match the functionality of the vertebrate retina, has provided new opportunities for vision systems and processing through the realization of new architectures. Research in both retinal cellular systems and nanodriven memristive technology has made a challenging arena more accessible to emulate features of the retina that are closer to biological systems. This paper synthesizes the signal flow path of photocurrent throughout a retina in a scalable 180-nm CMOS technology, which initiates at a 128 × 128 active pixel image sensor, and converges to a 16 × 16 array, where each node emits a spike train synonymous to the function of the retinal ganglionic output cell. This signal can be sent to the visual cortex for image interpretation as part of an artificial vision system. Layers of memristive networks are used to emulate the functions of horizontal and amacrine cells in the retina, which average and converge signals. The resulting image matches biologically verified results within an error margin of 6% and exhibits the following features of the retina: lateral inhibition, asynchronous adaptation, and a low-dynamic-range integration active pixel sensor to perceive a high-dynamic-range scene.**

***Index Terms*— Artificial retina, memristor, neuromorphic vision, sensor systems, silicon retina.**

I. Introduction

PERFORMANCE and efficiency requirements of bioprocesses and bioprocessing have set a challenging standard for researchers and engineers due to their seemingly insurmountable and extremely demanding specifications [1]–[4]. Neuromorphic computing is a powerful illustration of this paradigm, the foundation of which was formulated in [7], whereby large-scale adaptive analog systems were conjectured to be highly robust and power efficient. If neuronal activity and cellular connectivity can be experimentally verified and accurately modeled, then the hardware mapping of various biological systems can realistically be made possible. The focus of this paper is the vision system, where at present, restoration of sight to patients deprived of functional vision by degenerative receptors is thus far dependent upon the electrical stimulation of the surviving retinal cells [8]. This method lacks a correlation between the stimulus and the cellular processes within the retina, which results in only very limited vision being restored. The development of a successful prosthesis hinges upon improved predictive models based on the natural flow of signals in the retinal network.

A prerequisite for hardware mapping of retinal-based vision systems is the need to understand the structure of the retina in terms of the cellular connections and photocurrent processing. The retina has five layers: photoreceptor cells (outer boundary), horizontal cells, bipolar cells, amacrine cells, and ganglion cells (inner boundary). The bioarchitecture is shown in Fig. 1. When light enters the eye, it encounters two types of photoreceptors: the rod cells (approximately 120 million in number) and cone cells (approximately 6 million), which convert light into nerve signals. The relativity of these numbers becomes significant when one ventures into hardware mapping [9]–[15].

As noted, successful development of a retinal model requires experimental validation of the processes that occur within the retina. Over the past 50 years, experimental techniques have matured significantly, providing an adequate insight into the bioprocessing that takes place within individual retinal cells. Despite this, the absence of appropriate nanoscale circuit devices has impeded the development of smart imaging systems based on the retina. With device scaling of CMOS technology [19], and the recent progress and increased confidence in the manufacturability of memristors, such a nanocircuit element has created a new design domain for dense architectures. The memristor, postulated in 1971 by Chua [20] and fabricated for the first time by Hewlett-Packard [21], has paved the way for emulating complex biological functions and achieving the biomimicry of observed synaptic plasticity in neuronal systems [22], [23]. The nonlinear and adaptive response of memristors allows practical realization of complex synaptic connections [24], [25].

Manuscript received September 3, 2017; revised March 1, 2018; accepted April 20, 2018. Date of publication May 7, 2018; date of current version November 30, 2018. This work was supported in part by the National Research Foundation of Korea Grant funded by the Korean Government under Grant NRF-2017R1D1A1A09000613, in part by the DFAT Australia–Korea Foundation under Grant AKF00640 and Grant UWA RCA 2017, and in part by iDataMap Corporation. *(Corresponding author: Jason Kamran Eshraghian, Jr.)*

J. K. Eshraghian, Jr., C. Zheng, H. H.-C. Iu, and W. Lei are with the School of Electrical, Electronic and Computer Engineering, The University of Western Australia, Crawley, WA 6009, Australia (e-mail: jason.eshraghian@uwa.edu.au; ciyan.zheng@research.uwa.edu.au; herbert.iu@uwa.edu.au; wen.lei@uwa.edu.au).

K. Cho and M. Nam are with the College of Electrical and Computer Engineering, Chungbuk National University, Cheongju 362763, South Korea (e-mail: krcho@cbnu.ac.kr; minhonam@cbnu.ac.kr).

K. Eshraghian is with iDataMap Corporation Pty Ltd., Eastwood, SA 5063, Australia (e-mail: keshraghian@idatamap.com).

Color versions of one or more of the figures in this paper are available online at http://ieeexplore.ieee.org.

Digital Object Identifier 10.1109/TVLSI.2018.2829918

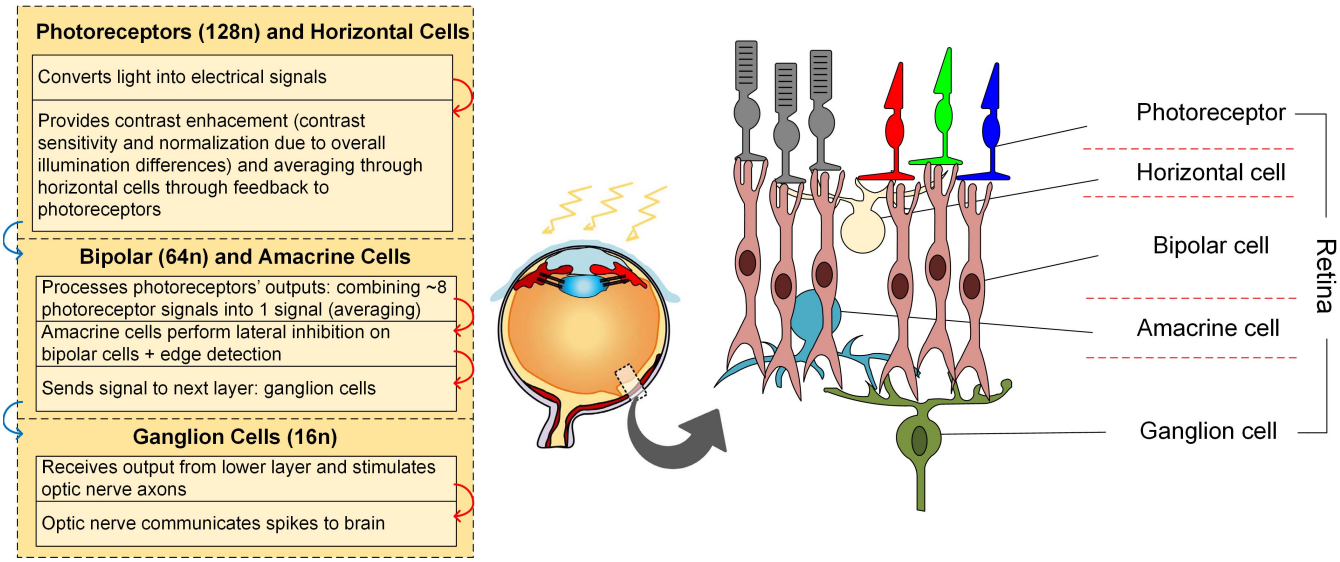

Fig. 1. Retinal bioarchitecture adapted from [16] and [17]. Photoconduction pathway for ionic current flows through photoreceptor cell → horizontal cell → bipolar cell → amacrine cell → ganglion cell, and then to the visual cortex. Bipolar and amacrine cells transfer electrical signals from photoreceptors to the ganglion cells. Lateral connections involve both horizontal and amacrine cells and span throughout the OPL and the IPL. Amacrine cells are responsible for further processing the retinal image. Ganglion cells receive electrical signals from the bipolar and amacrine cells. Ganglion cells process electrical signals for the optic nerve and spike at a faster rate if there is a change in the overall light intensity for a group of photoreceptors, sending a signal to the visual cortex via the optical nerve. Roughly 100 photoreceptor outputs are capable of contributing to a single ganglion cell [22]. Amacrine cells are responsible for 70% of the ganglionic layer input [18]. The proposed three-level architectural mapping depicts the functions needed for mapping into hardware, where n is the scaling factor. The first layer involves photoreceptor and horizontal cells; the second layer includes amacrine and bipolar cells, while ganglion cells form the third and final layers.

The research motivation arises from the lack of any existing circuits, which achieve not only an adaptive image output but also performance at a cellular level in the same manner as the retina. Present circuits aim to achieve neuromorphic vision by producing functional images through, for example, edge detection and averaging methods, at a higher level, without regard to cellular-level currents and action potentials occurring within the retinal cells [26]. This paper proposes an approach that treats each pixel as an output cell, thus designing a retinal-inspired circuit that captures the signal flow of photocurrent passing through the cellular layers, with each subcircuit constrained in size to depict the ratio of cells that are present in the retina. The signal initiates at a 128×128 memristor-CMOS active pixel sensor (APS), which represents the photoreceptor cells with hexagonal memristive interconnects that emulate the effects of lateral inhibition and averaging, often associated with the function of the horizontal and amacrine cells [18]. The output signals converge to a 64×64 memristive network of ON/OFF-bipolar cells, which respond with a graded potential mediated by interconnecting amacrine cells. The signal yet again converges to a 16×16 network of amplitude-to-frequency converters, which perform the functionality of the output ganglion cells, with each node in the array emitting a spike train, which approximates the signal sent through the optic nerve to the visual cortex for image interpretation in the brain. Alternatively, this signal can be quantized by its frequency and has a bit assigned in order to generate an output image. This ultimately achieves an asynchronous adaptive response image sensor, which not only models scalable retinal behavior at a cellular level but also reduces power consumption as compared to other retinal chips and microprocessors while maintaining an acceptable error bound of 6%. Memristors have been shown to be stochastic in nature, which gives rise to cycle-to-cycle variations within the same device. As the cellular processes that are dealt with in this paper (such as graded potentials and spiking) occur on the order of milliseconds, as a physical device, a neuromorphic vision circuit that operates at the level of cellular processing proves to be highly robust to nanosecond variations [27].

The various components of the image processing circuit each perform a separate function contributing to the overall artificial retina architecture, as inspired by the various cells within the retina. As such, this paper will follow a bottom-up approach in presenting our results, which first focuses on the individual cellular circuits before presenting them as a network. Section II provides a basic framework of the retina from a cellular perspective with a focus on functionality arising from the underlying ionic current gating theory formulated by Hodgkin and Huxley (HH) [28]. A brief explanation and justification of the functions of each cell to be mapped into hardware are described. For convenience, memristor theory is highlighted in Section IV to justify the rationale in its adoption in our architecture with a description of the model used in this paper. Section V presents the constituent cellular circuits, which are combined and structured into a larger network in Section V as a 3-D array, which is able to process continuous signals, initiating at the photoreceptor, through to the output ganglion cell. The full network is simulated in Section VI with appropriate comparisons made against prevalidated experimental data. Experimental results

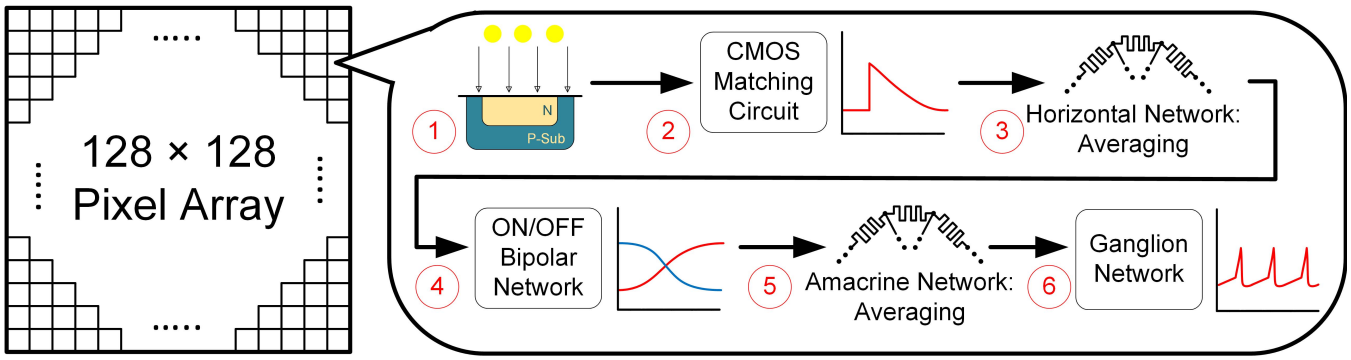

Fig. 2. High-level architecture and signal flow of the retina-based image sensor. Each cellular layer is modeled independently. 1: photoreceptor cells with a memristor-CMOS integration type APS. 2: supplementary matching circuit to perform adaptive imaging. The signal output passes through to 3 a memristor-based horizontal cell network to average and smooth the signal from various photoreceptors. Note that the signal is not passed through a single memristor, but through a horizontal network as described in Section IV-B and in Fig. 6. This averaged signal is passed onto 4 a CMOS ON/OFF bipolar cell network for further processing, before being averaged once again in 5 a memristor-based amacrine cell network. The output is finally passed onto 6 a CMOS ganglion cell network. The system comes together to mimic the functionality and image processing capabilities of the retina, and the spike train output from the ganglion cell can either stimulate the optic nerve for interpretation by the visual cortex, or each frequency value can be assigned a bit to construct an image a computer can comprehend. The architecture presented represents a single signal flow pathway, in contrast to Fig. 3 which depicts the interconnections between various signal flow pathways connected by horizontal cells, amacrine cells, and chemical and electrical synapses.

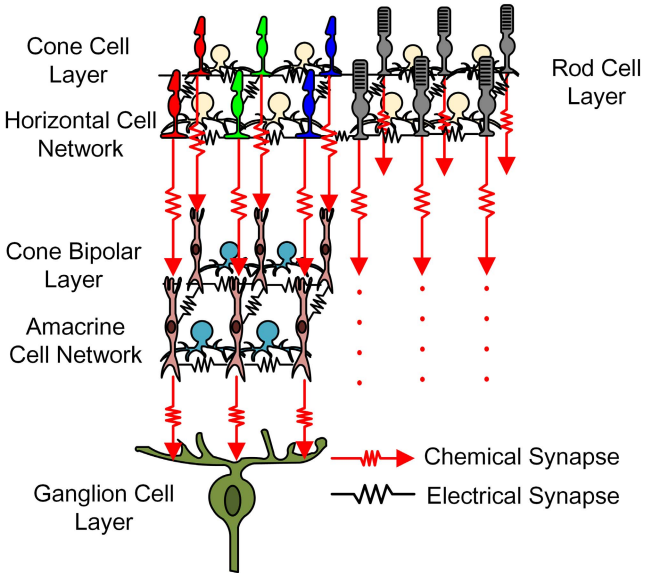

Fig. 3. Proposed scaled-down architectural platform derived from a retinal network model in [29], illustrating the foundational building blocks of the 3-D architecture, this paper proposes for future system-on-chip implementation. Many of the neurons in the retina, photoreceptors, horizontal, and bipolar cells communicate through passive gap junctions rather than through spikes. The cone cell pathway to the ganglion cell layer via the cone-bipolar layer interacts vertically with chemical synapses and laterally (via horizontal and amacrine cells) with electrical synapses.

are also provided, which serve to illustrate functionality of the proposed architecture of the quantized spike train in the form of a real image output.

II. Biological Model

Transformation of the architecture shown in Fig. 1 into the signal processing model shown in Fig. 2 that could overcome space-power-speed constraints with current technological limitations appears impractical. However, a scaled-down version is feasible by the way of memristor-CMOS technologies. To alleviate complexity in the simulation and verification of bioflow, we have streamlined the photoreceptor cells to focus on the cone cell pathway. As such, this section serves as a brief introduction of the retina and is not to be read as a thorough review. More in depth information can be found in [30]–[32]. Fig. 2 presents the architecture of the signal flow from the perspective of a single pixel. The development of a full retina requires interconnections between many signal flows, but before moving onto that task in Section IV, the function of each constituent cell is described.

A. Photoreceptor Cells

Rod and cone cells essentially act as transducing elements by transforming the incident light stimuli into an electrical photocurrent. The magnitude of the voltage change in the cell membrane is proportional to the logarithm of the intensity of light [33]. Rods initiate vision under low scotopic light levels of illumination ($10^{-3} - 10^{-6}$ cd/m^2), while cone cells initiate under high photopic light ($10 - 10^{8}$ cd/m^2) [30].

Given there are approximately 20 times as many rod cells present in the retina as there are cone cells, this suggests we think of the signals from many of these rod cells as converging together to improve the signal-to-noise ratio (SNR) under low light levels rather than for enhanced visual acuity. As such, this paper will focus on the cone cell signals, even though many of the features of the circuit are also adaptable to rod cells. HH biokinetic modeling can be used to describe the system of ionic currents and gating variables within each cell, but for the purposes of the development of a VLSI of a network of photoreceptor cells, we are more interested in the interaction of photoreceptors between one another as opposed to the intrinsic cellular processes. The outputs of the photoreceptor cells form synaptic connections with bipolar cells and horizontal cells.

B. Horizontal Cells

Horizontal cells form synaptic connections between photoreceptors and bipolar cells. Via the horizontal cells, lateral connections with neighboring groups of photoreceptors and bipolar cells are made. These can be conceived as being a resistive layer spanning the outer plexiform layer (OPL) of the retina, with the architecture allowing dynamic-range adjustments. The strength of the electrical potential depends on the physical proximity with the photoreceptor, where photoreceptors hyperpolarize the nearby horizontal cells, and distant horizontal cells are depolarized due to lateral inhibition [34].

C. Bipolar Cells

Bipolar cells behave as the signal couriers between the photoreceptors that react to light stimuli and the ganglion cells that carry these signals out of the retina. Bipolar cells process visual signals through the integration of analog signals generated by synaptic currents and (nonspike generating) voltage-gated membrane currents. There are two functional types of bipolar cells: ON-center and OFF-center cells. Photoreceptors release only one neurotransmitter, glutamate, yet bipolar cells react to this stimulus with two different responses, ON-center (glutamate release via photoceptor depolarization) and OFF-center (glutamate release via photoreceptor depolarization). ON-cells respond to the onset of light and OFF-cells respond to the cessation of light, and these are thus complementary in nature—an important consideration when translating this particular feature into a circuit.

D. Amacrine Cells

Amacrine cells exist in the inner plexiform layer (IPL) and give transient light responses to signals from both ON- and OFF-bipolar cells. They can be classified into sustained and transient cells: sustained amacrine cells obtain their inputs from the bipolar cells that are not inhibited by other amacrine cells. The response of sustained amacrine cells then inhibits bipolar terminals in the narrow field region, causing those terminals to respond transiently. Essentially, this network of amacrine cells forms a high-pass filter of the bipolar signal that enables the detection of moving edges [35].

E. Ganglion Cells

Ganglion cells send the output of the retinal signal to the optical nerve, and by extension, to the visual cortex. They convert graded potential inputs from bipolar cells into action potentials—a sequence of spikes transmitted to be interpreted by the brain. The frequency of firing is related to the magnitude of the stimulation [36] and provides a measure of the difference in intensity between the center and surround region of its receptive field. Increasing the intensity in the center region increases the firing rate of ON-center ganglion cells, while an increase of the OFF-center cells signals a rapid decrease in light intensity on the center of the receptive field.

The adaptation of such cells and neural processes into circuits requires significant advancement in the field of synthetic biology, and the advent of the memristor proposes a new method of being able to inch closer toward meeting the golden standard of design specifications.

III. Ideal Memristor Model

The memristor is a fundamental circuit element due to the constitutive relationship it holds between charge and flux. Note that even though q and ϕ are referred to as charge and flux, they are not necessarily associated with real physical charge and flux (as exhibited in classical conductors and inductors) [37]. Additionally, the integral relationship between voltage and flux allows a memristor to retain history and potentially have different values of current for a given voltage. As a result, the memristor allows for different values of resistance despite being excited by identical voltages, due to it being a function of historical voltage. This gives rise to the nomenclature surrounding the memristor, a portmanteau of "memory resistor." The intrinsic nonlinearities and polarity dependence of the individual memristor give rise to many more configuration permutations than the same number of other fundamental circuit elements, namely, the resistor, capacitor, and inductor. The behavior of memristors connected serially, in parallel and via coupling, is theoretically and experimentally evaluated in [38] and [39], and by taking advantage of their composite connections, it is anticipated that networks with a density of 100 billion synapses/cm^2 in each layer should soon be possible by shrinking memristors down to 30 nm across. This implies that highly dense 3-D structures with a very large number of memristors within very close proximity of one another can be made possible—precisely the requirements of neural modeling.

Ideal memristors can be classified into either charge controlled or flux controlled [20]. The relationship between current and voltage of a charge-controlled memristor is expressed by

$$V(t) = M(q)i(t) \tag{1}$$

where t is the time, $V(t)$ is the voltage, q is the charge, and $M(q)$ is the memristance. In its derivative form, memristance can be defined as

$$M(q) = \frac{d\phi(q)}{dq} \tag{2}$$

where ϕ is the flux—the time integral of voltage $v(t)$. Contrastingly, the current of a flux-controlled memristor is

$$i(t) = W(\phi)v(t) \tag{3}$$

where $W(\phi)$ denotes flux-controlled memductance and can be derived from (2) as

$$W(\phi) = \frac{dq(\phi)}{d\phi}. \tag{4}$$

Flux ϕ and charge q are two intrinsic state variables affecting memductance, which is a characteristic embedded into the memristor at the time of fabrication. The memristive array in Sections IV–VI. utilizes a memristor with a linear piecewise charge-flux curve, resulting in a flux-controlled switching memristor, as presented in [37]. This implies that there are two possible memristance states, M_{ON} and M_{OFF}, which

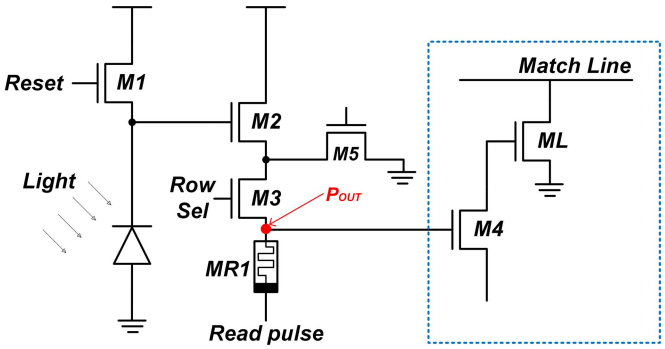

Fig. 4. Photoreceptor cone cell circuit: photodiode current can be stored within memristor MR1, and adaptive vision is emulated by matching current light input to the prior state of stored light. This mechanism is embedded through transistors $M4$ and ML, whereby the potential at the gate of $M4$ is only altered [and thus, the internal state x of MR1 as represented by (5)] if the match line differs by a value greater than the transistor threshold from the present input. That is to say, power is only dissipated in the circuit when there is a change of light input, thus emulating adaptive functionality of the photoreceptor cell. The output of the circuit is P_{OUT}, denoting photoreceptor cell output.

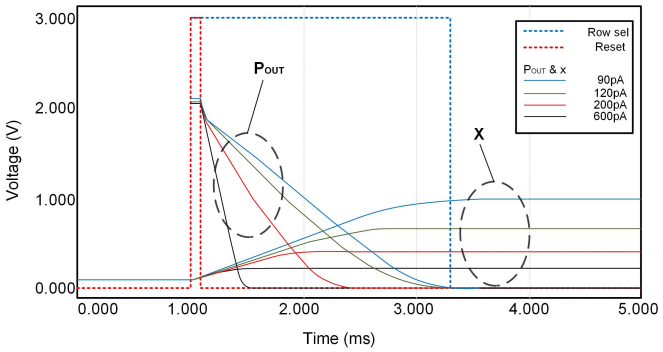

Fig. 5. Photoreceptor cone cell simulation: voltage response at output P_{OUT} and the internal state of MR1, x, upon injecting photocurrents of various values representing various light intensities. The biological cone cell response to a photocurrent injection is biphasic—this is not shown in the single cell simulation [30]. Instead, biphasic behavior is emulated once the full network of cone cells is combined with appropriately biased memristors. The storage ability of the cell model is shown to saturate beyond photocurrents of 600 pA, which is well above the value verified by experimental data [40] allowing this model to capture the full range of photocurrents which can be translated into meaningful images at the visual cortex.

correspond to the memristor exhibiting a high state or a low state, respectively. In theoretical circuit analysis, this can sometimes be approximated to an open circuit and a short circuit, thus being referred to as a "memristive switch." This paper utilizes an ideal switching memristor in the horizontal and amacrine cell circuitry, and a generic memristor in the photoreceptor cell circuitry. The characterization of the generic memristor is provided in Section IV.

IV. Retinal Cell Circuit Models and Simulations

The constituent circuits for each component of the retinal cellular pathway are presented in this section to validate the building blocks of the architecture, before being scaled into a full network simulation in Section V.

Here, each cell is simulated independently of one another to verify their functionality. The CMOS technology is produced using the 180-nm process devised by SK Hynix, with information regarding scalability in Section V.

A. Photoreceptor Cell Circuitry

The proposed circuit for a single photoreceptor cone cell at the front-end interface of the retina is shown in Fig. 4, with accompanying simulations in Fig. 5 showing voltage response at output P_{OUT} and internal memristor state x as a function of input photocurrent.

Upon the incidence of light, the output P_{OUT} displays a graded potential which is stored by the memristor MR1 according to the state equation

$$x = \frac{M_{\mathrm{OFF}} - M_{\mathrm{INITIAL}}}{M_{\mathrm{OFF}} - M_{\mathrm{ON}}} \tag{5}$$

where M_{INITIAL} is the initial memristance of MR1 and x is its intrinsic state variable. This represents a generic memristor, the internal characteristics of which are dependent upon the ratio between the difference between initial resistance and the ON-state resistance, with the OFF-resistance value. The initial memristance is dependent upon photocurrent which controls $M2$ of Fig. 4, and changes the node voltage of P_{OUT}. The time-dependent variation of x, dx/dt, is identical to $dV_{P_{\mathrm{OUT}}}/dt$, which is $M_{\mathrm{INITIAL}} \times (di/dt)$, otherwise known as current-induced charge q incident upon the photodiode. Thus, dx/dt corresponds to the photocurrent on the photodiode, and x is varied by photocurrent and the integration time based on the amount of charge q. The bordered segment of the circuit in Fig. 4 represents a detection unit, whereby the match line allows for the detection of the current from a previous point in time. The signal is only passed where a change in current is detected. This is used to mimic adaptive perception in the retina. At steady-state illumination, the output will only react to changes in light illumination, thus replicating retinalike behaviors.

B. Horizontal Cell Circuitry

It has been shown in [26] that memristive networks perform better than resistive grids for edge preservation smoothing. Additionally, using switching memristors characterized by (3) and (4) in Fig. 6 results in behavior that significantly mimics neuronal action potentials when injected with a short rectangular pulse of photocurrent into the input nodes. The network of memristors performs not only functional averaging, but additionally mimics depolarization and hyperpolarization. This is illustrated in the simulation shown in Fig. 7. Upon the injection of six photocurrent responses, their currents are averaged through the memristor network. The state of a charge-controlled switching memristor is dependent on the time integral of current flowing through it as implied by (1) and (2). Once the charge exceeds a certain threshold (as determined by the device itself), the internal state of all adjacent memristors will switch ON (approximated to an open circuit in circuit analysis) and allows the full output of P_{OUT} from the photoreceptor circuit to momentarily pass through. The final phase or segment "5" on the curve represents

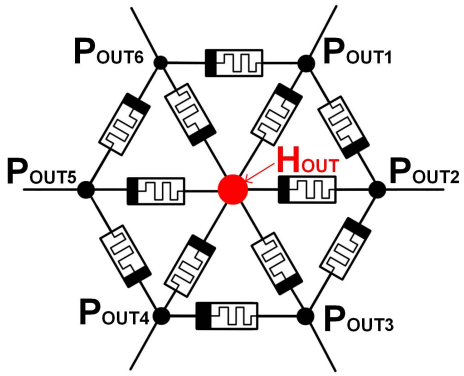

Fig. 6. Horizontal cell circuitry: the equivalent representation of the horizontal cell network which allows for lateral communication between photoreceptor cells via memristors. Each node along the perimeter of the hexagon (depicted as a circle) provides inputs from the photoreceptor outputs $P_{\mathrm{OUT1}\rightarrow 6}$ of Fig. 4 (otherwise can be referred to as the horizontal cell inputs $H_{\mathrm{IN1}\rightarrow 6}$). The central node H_{OUT} (horizontal cell output) emits a signal of six averaged photoreceptor responses to the next cell circuitry for processing. An alternative 3-D representation can be found in Fig. 12. The memristor used in this model is the switching memristor characterized by (4) and (6). The memristors have been oriented with alternating polarities, and assuming all memristors in the system are initialized at the origin of their odd-symmetric flux-charge curves, this will result in closer emulation of cell behavior by likening the voltage response (see current output for voltage-controlled ideal memristors) to the action potential curve of cells. More specifically, with respect to Fig. 7, the slope between positions "1" and "2" becomes steeper and more consistent by alternating the polarities of memristors within each branch.

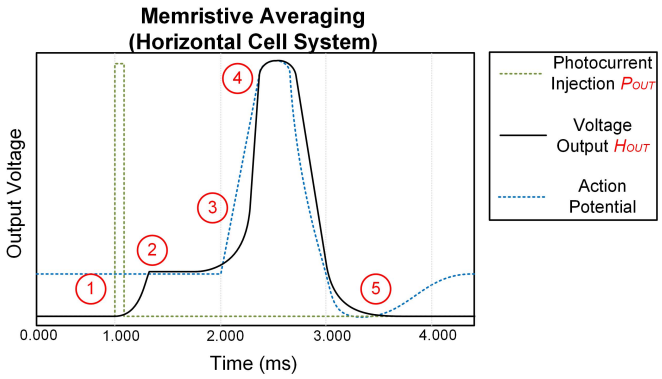

Fig. 7. Horizontal cell simulation: voltage output at P_{OUT} of Fig. 4 when behaving in a network as in Fig. 6, and is subject to a pulse of photocurrent injection. The photocurrent is injected into a single cone cell circuit, while neighboring cone cells (connected via memristors) are left without stimulation. The linear relationship between voltage and resistance means the action potential is scalable. As such, the voltage axes have remained unlabeled—the important note is that the voltage at "2" is 1/6 of the value at "4" due to the adjacent memristors simultaneously switching ON, which mitigates the spread of photocurrent throughout the network. The branches with the least total resistance will see greater charge flow, and thus, central-node memristors will switch states faster than branches with greater resistance. Depending on the value of photocurrent injection, branches with total resistances about a given amount will fail to switch, which corresponds to point "4." Without further photocurrent input, the circuit hyperpolarizes and goes back to its resting state. Thus, the voltage potential strongly resembles the shape of an action potential of a neuron when triggered, which has been overlaid on the simulation result for comparison.

the refractory period of the neuron: the phase in which it recovers before producing another action potential. This is for the simplest case of all memristors initially being switched OFF and there is a short photocurrent pulse injection at the photoreceptor layer for any nonedge pixel.

From a circuit's perspective, in a circuit where the hexagonal circuit is connected in a network with a large number of other hexagonal circuit, the branches with the least total resistance (i.e., a lower number of memristors) will have memristors that switch states faster than those with greater resistance (i.e., a greater number of memristors). As a comparatively greater current (and, therefore, total charge) flows through the pathway with least resistance, this results in the memristor that directly connects each input node to output node switching before any other memristor in the network (as denoted by the sudden flattening of the curve at point "2"). Following that, memristors in branch pathways with increasing total branch resistance are sequentially switched. Higher order branches with resistances above an amount dependent upon the photocurrent input will fail to switch due to insufficient charge/current flow—this corresponds to point "4," where all other memristor branches cease to switch, and the photocurrent input goes back into the resting state causing the drop back to "5." In terms of averaging, the instantaneous current that passes through the output node when there is only one input can be calculated to be $I_{H-\mathrm{OUT}} = (1/6)I_{P-\mathrm{OUT}}$, and by superposition, the instantaneous current total at the output node of each hexagon is approximately the average of all current inputs for the six input nodes. Caution must be taken with the superposition principle, as it will only result in correct calculations for instantaneous measurements in this circuit.

Averaging multiple photocurrents and exposures reduces noise without compromising details. This is because it increases the SNR of the incoming image. It may also increase the bit depth of images, which means the memristive network presented is able to increase the dynamic range of images received by low-dynamic-range sensors. When all memristors in Fig. 6 are set to "OFF," then current flow is not impeded and the signals undergo a first stage of averaging before being passed through to the bipolar cell array. The hexagonal structure depicted in Fig. 6 is tessellated across the network to produce the photoreceptor-horizontal cell-OPL layer, and each circuit represents one pixel. Therefore, the hexagonal structure takes the input of six photoreceptor pixels. Any leakage of current beyond the first-order branches throughout the system is insufficient to switch the state of any memristors other than those that are directly adjacent to the node receiving photocurrent. This is due to the large amount of current division that occurs across the many nodes of the system.

The memristors in Fig. 6, with associated simulation results given in Fig. 7, are based loosely on the ideal memristor demonstrated in [37], and adapted so as to have ON- and OFF-resistance values more appropriate for ionic channeling

$$q(t) = w(t)(0.2\phi(t) + 400|\phi(t) + 0.25| - 400|\phi(t) - 0.25|) \quad (6)$$

which is an odd-symmetric piecewise linear function physically equated to an ideal switching memristor with $M_{\mathrm{ON}} = 5\ \Omega$ and $M_{\mathrm{OFF}} = 0.001\ \Omega$, and $w(t)$ is based on a form of the Joglekar window function from [41] which we have adapted

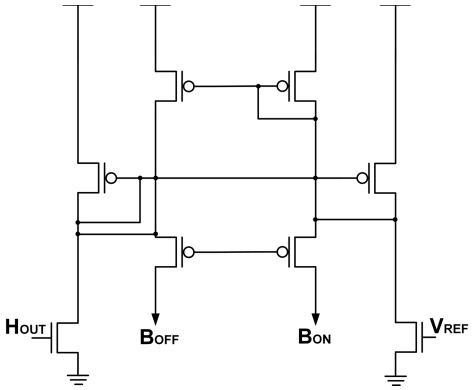

(a)

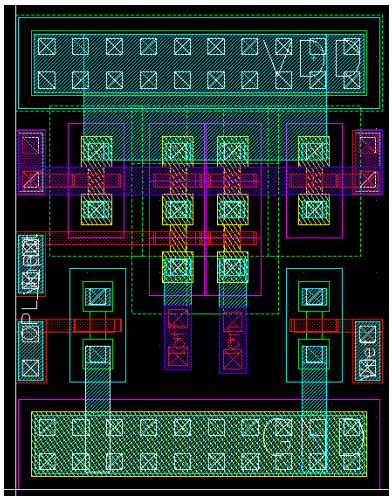

(b)

Fig. 8. Bipolar cell circuitry: the bipolar cell circuit generates "ON" and "OFF" responses that vary in accordance with the intensity of light adapted from [45]. The threshold between "ON" and "OFF" current is controlled by the reference voltage V_{REF}, which is predetermined from biological data. If input current from the horizontal cell output H_{OUT} (or otherwise, the bipolar cell input B_{IN}) is greater than the threshold, $I_{B_{\mathrm{on}}}$ flows: $I_{B_{\mathrm{ON}}} \propto I_{H_{\mathrm{OUT}}} I_{\mathrm{TH}}$, where I_{TH} is threshold current and $I_{H_{\mathrm{OUT}}}$ is the current response from the horizontal cell circuitry, namely, the output from the central node in Fig. 6. $I_{B_{\mathrm{OFF}}}$ is represented by $I_{B_{\mathrm{OFF}}} \propto 1/I_{H_{\mathrm{OUT}}}$ when the condition $I_{H_{\mathrm{OUT}}} < I_{\mathrm{TH}}$ is created by V_{REF}. (a) Bipolar cell circuit schematic. (b) Bipolar cell circuit layout.

to be applicable to modeling the influence of nonlinear drift and boundary condition on an odd-symmetric ideal memristor

$$w(t) = 1 - 2x^{2p} \tag{7}$$

where p is a positive integer that varies the boundary ramp and is set to $p = 10$. It is important to note that the flux-dependent memristors are not restricted to devices with specific mechanisms and typically use physical mechanisms by using a measurable quantity as the state variable of the device similar to the approach presented in [42] and [43]. Models based on physical devices, such as that presented in [44], can still be implemented into this architecture, provided that the specific parameters are selected to ensure a sufficient ON–OFF memristance ratio and a low enough memristance variation while switched ON.

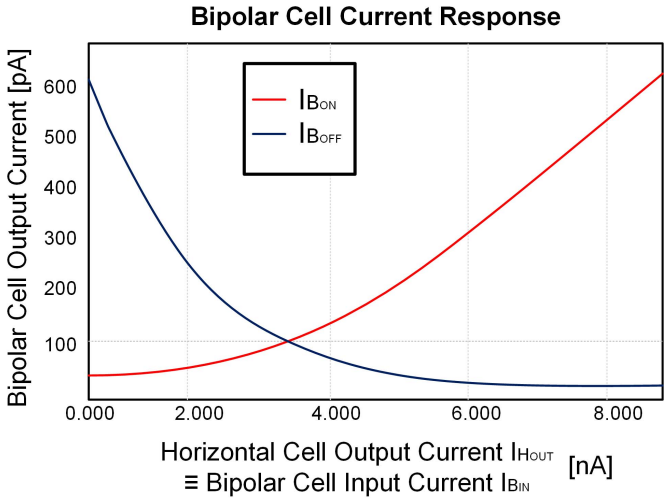

Fig. 9. Bipolar cell simulation: a single bipolar cell circuit responds with both ON- and OFF-center currents. While the input current from the horizontal cell output H_{OUT} increases, the current output at B_{ON} increases and B_{OFF} decreases. Biologically determined results of inverse proportionality between B_{ON} and B_{OFF} confirm the validity of the simulations of the bipolar circuit model.

C. Bipolar Cell Circuitry

The two types of bipolar cells, ON-center and OFF-center bipolar cells, are merged into the same schematic, as shown in Fig. 8(a), adapted from the 1-D version presented in [45], with the simulation results of Fig. 8(b) displayed in Fig. 9. The circuit generates two types of responses according to light intensity, and the threshold between the ON and OFF current is controlled by an external voltage V_{REF}, which can be predetermined using biological data.

For the ON-bipolar cell response $I_{B_{\mathrm{ON}}}$, $V_{\mathrm{DD}} = 1.8$ V, $V_{\mathrm{TH}} = 0.4$ V, $V_{\mathrm{BQ}} = 1.4$ V, $V_{\mathrm{REF}} = 0.9$ V, and the outputs B_{OFF} and B_{ON} are both connected to 47-fF capacitors.

The response of both $I_{B_{\mathrm{ON}}}$ and $I_{B_{\mathrm{OFF}}}$ fits the experimental data of bipolar cells [46] as graded potentials, confirming the validity of the circuit.

D. Amacrine Cell Circuitry

The amacrine cell network operates in much the same way as the horizontal cell network presented in Section IV-B, characterized by the ideal memristor generically modeled by (4), (6), and (7). Six bipolar cell signals converge and are averaged with memristors (using the method in Fig. 6), as a simplified functional model of the amacrine cell, and produce the input for a single ganglion cell circuit. Each node of the hexagonal circuit forms a single "pixel" in the ganglion cell network. The main difference between the amacrine cell circuit and the horizontal cell circuit is that there are two separate layers of amacrine cells, one which sees input only from various B_{OFF} nodes and one which sees inputs only from B_{ON}. Instead of P_{OUT} photoreceptor outputs (as in Fig. 6), we see B_{OFF} and B_{ON} as the inputs, and central node cell outputs of A_{OFF} and A_{ON}, respectively. Akin to our photoreceptor layer, the memristors in this layer are intended to mimic some of the properties of amacrine cells, thereby allowing a means

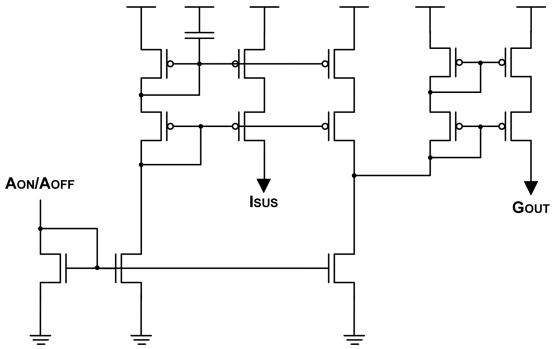

(a)

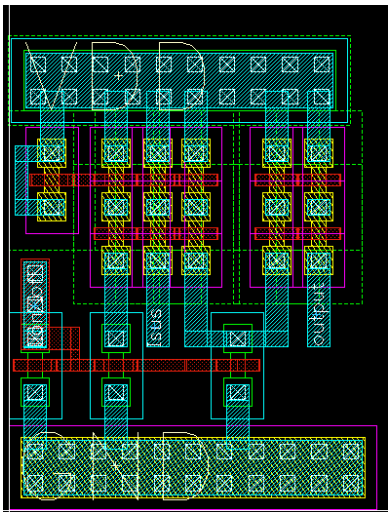

(b)

Fig. 10. Ganglion cell circuitry: the ganglion cell circuit adapted from [45] will receive its input from either ON- or OFF-center bipolar/amacrine cells depending on whether it is either an ON-center or OFF-surround ganglion cell [47]. An ON-center cell is activated when the center of its receptive field is exposed to light, and is otherwise inhibited when the surrounding area is exposed to light. OFF-surround ganglion cells have the opposite reaction. Our model of the ganglion cell does not produce both ON-center and OFF-surround signals from the one circuit, and is instead dependent on whether it receives $I_{B_{ON}}$ or $I_{B_{OFF}}$ from the bipolar cell. In our simulations of the ganglion cell, we only use I_{ON} as the input to the circuit. The output current $I_{G_{OUT}}$ is sent to through the optical nerve so an image can be interpreted by the visual cortex of the human brain, or alternatively can be passed through an analog-to-digital converter to assign a bit value to the signal so as to represent a brightness value. (a) Ganglion cell circuit schematic. (b) Ganglion cell circuit layout.

to detect changes in moving edges and the implementation of a form of center–surround interaction that contributes to the resulting response properties of the final ganglion cell pixel.

E. Ganglion Cell Circuitry

The circuit shown in Fig. 10 adapted from [45] generates sustained responses and transient responses, I_{SUS} and $I_{G_{OUT}}$, respectively, of the input current. The sustained output current I_{SUS} is low-pass filtered by a current mirror with a capacitor, and the transient output current $I_{G_{OUT}}$ is high-pass filtered by subtracting the low-pass-filtered input from the input current. Therefore, this circuit can simulate four types of ganglion cells: ON and OFF sustained and ON and OFF transient ganglion cells.

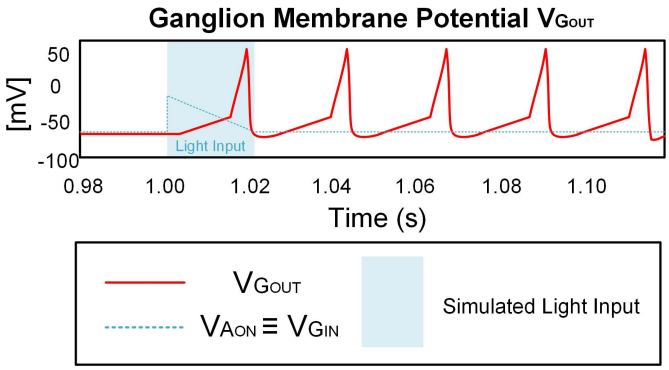

Fig. 11. Ganglion cell simulation: simulation of a single ganglion cell circuit from Fig. 8. When $V_{A_{ON}}$ is changed (logically equivalent to the ganglion cell input $V_{G_{IN}}$), the voltage at G_{OUT} and $V_{G_{OUT}}$ produces a spike train.

For the simulation of transient ganglion cell voltage response $V_{G_{OUT}}$ shown in Fig. 11, a graded potential is applied at the input $V_{A_{ON}}$, and $V_{DD} = 1.8$ V, $V_{TH} = 0.4$ V, and the output of the ganglion cell is connected to a 47-fF capacitor. Importantly, the response of the ganglion cell $V_{G_{OUT}}$ is a spike train, also displayed in the simulation results shown in Fig. 11, and thus matches biological data of the ganglion cell.

Each of the cell circuitries mentioned operates in a sequential flow, starting at the photoreceptor cell, with the final output at the ganglion cell circuit. Simulations of this circuit are provided in Section V in the context of the full pathway (from photoreceptor injection to ganglion cell output) to confirm biological accuracy.

V. RETINAL NETWORK MODEL

The undue complexity of neural processes, such as retinal image processing and each associated cellular circuitries, has been described in Sections I, II, and IV. For ease of understanding, a summary of the signal that flows through each cell has been provided below, prior to discussing how the circuits are combined to produce a cellular network.

1) The photoreceptor cell is a CMOS APS circuit, which passes a signal from P_{OUT} to the horizontal cell circuit.
2) The horizontal cell is a hexagonal array of memristors, where each hexagon accepts six separate signals from $P_{OUT_{1\to6}}$ and averages them with memristors. This signal is passed onto the bipolar cell circuit.
3) The bipolar cell is a CMOS circuit which generates two outputs, representing the two types of bipolar cells that exist in nature: the ON-center and OFF-center bipolar cells. These correspond to B_{ON} and B_{OFF}, which pass signals onto the amacrine cell circuit.
4) The amacrine cell, much like the horizontal cell, is a hexagonal array of memristors. However, unlike the horizontal cell input, there are two different types of input sources: B_{ON} and B_{OFF}. Therefore, two separate layers of hexagonally connected memristor amacrine cell circuits diverge the two signals. Due to symmetry, and for the sake of simplicity, we focus here only on the ON-center bipolar cell input B_{ON}. Each amacrine cell

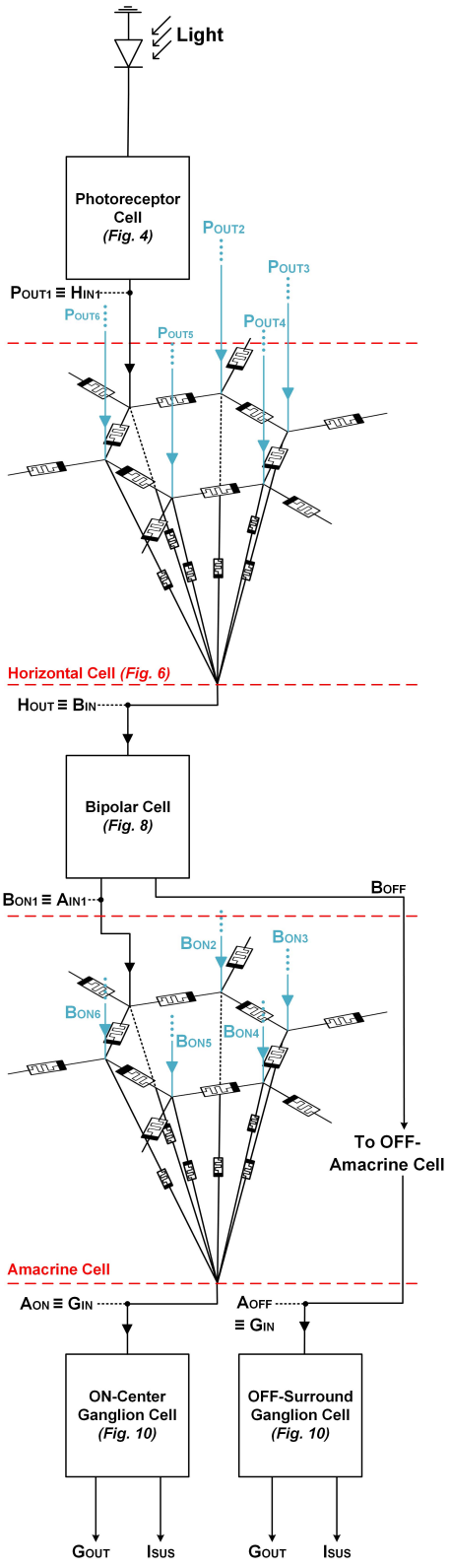

Fig. 12. Retinal network model: the signal flows through the retina initializing as light impinging upon the photoreceptor cell through to the ganglion cell output. Each light input can be represented by four different types of ganglionic output cells.

accepts six different signals from $B_{ON_{1\to 6}}$ and averages them, from which a single output A_{ON} is generated and passed to the ganglion cell input.

5) The ON-center ganglion cell is a CMOS circuit, which accepts an input from A_{ON} (conversely, OFF-surround ganglion cells accept A_{OFF}), and is high-pass filtered to generate the spike train output at G_{OUT}. This signal is the final output of the overall system and is sent to the visual cortex for interpretation.

The flow of photocurrent through a series of single cells is shown in Fig. 12.

In a practical device, the signal that flows through a series of single cells from photoreceptor → ganglion cell would correspond to a single pixel. Therefore, this section serves to extend out the photoreceptor cell circuit into a 128×128 array. The photoreceptor outputs $P_{\mathrm{OUT}_{1\to 6}}$ interact and average with their immediately adjacent cells in the horizontal cell memristor array. The averaged signal provides the input to the bipolar cell, which has been extended to a 64×64 network. Each signal is averaged with another six adjacent bipolar cell signals $B_{\mathrm{ON}_{1\to 6}}$ and thus provides the input to a 16×16 ganglion cell array. As such, our network simulates 16 384 photoreceptor cells, 4096 bipolar cells, and 256 ganglion cells in a single run. The relativity of these numbers is biologically significant, as signals from the initializing region of the retina converge together as they approach the brain—much like our hardware system. The pixel array representation of the network is shown in Fig. 13.

Each of the 256 ganglion cells will produce an output spike train, and the frequency of these spike trains corresponds to the light intensity of the image as perceived by the visual cortex.

VI. Experimental Results

A. Retinal Network Simulation Results

The CMOS circuit in Fig. 12 was designed using the SKHynix 180-nm process. As all circuits operate in the subthreshold region, a high supply voltage was not necessary. The CMOS photoreceptor and bipolar and ganglion cells were designed with $V_{\mathrm{DD}} = 1.8$ V, $V_{\mathrm{TH}} = 0.4$ V, $V_{\mathrm{BQ}} = 1.4$ V, and $V_{\mathrm{REF}} = 0.9$ V, and all outputs P_{OUT}, B_{OFF}, B_{ON}, and G_{OUT} are connected to $47fF$ capacitors. The minimum feature size of a transistor is $1.58\ \mu\mathrm{m} \times 0.78\ \mu\mathrm{m}$. As shown in the CMOS chip design in Fig. 14, the layout was arranged with 128×128 photoreceptor circuits, 64×64 bipolar circuits, and 16×16 ganglion circuits with a die size of 3 mm × 3 mm. The generic memristor used in the photoreceptor cone cell (see MR1 in Fig. 4) is simulated with a modified version of the HP TiO_2 memristor presented in [48] whereby the state equation is characterized with (5). The ideal memristor used in the horizontal and amacrine cell averaging system is based on the model presented in [49], where the charge-flux relationship is a piecewise linear function enabling perfect switching between resistance states $M_{\mathrm{ON}} = 5\ \Omega$ and $M_{\mathrm{OFF}} = 0.001\ \Omega$ at the threshold flux value of $\pm\Phi_T = 2.5$. The device parameters of the ideal memristor are loosely based on those from [49], where average carrier mobility $\mu_V = 10^{-10}\ \mathrm{cm}^2/(\mathrm{V{\cdot}s})$, device thickness $D = 10$ nm, and the device-dependent constant is $\gamma = -49.9 \times 10^9$. While the model presented in [44] is a better representation of oxide-based RAM, the memristor device in [49] was instead used in this paper to ensure an

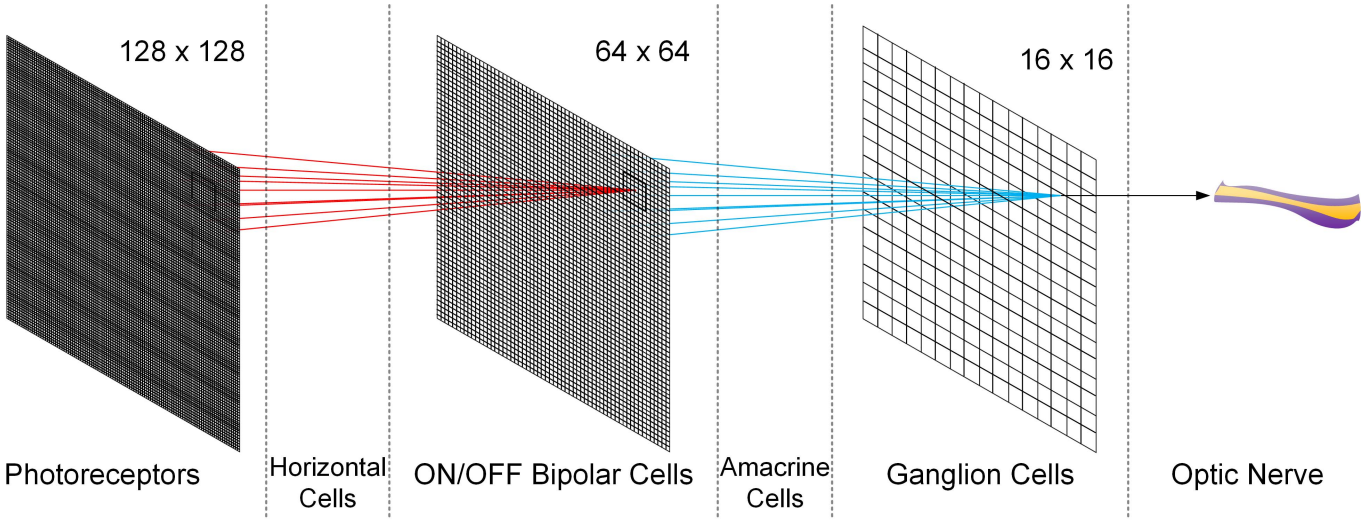

Fig. 13. Pixel array representation of the full signal flow convergence from a 128 × 128 array of photoreceptor circuits to a 64 × 64 array of bipolar cells and to a 16 × 16 array of ganglion cells. For clarity, the distance between the converging signals has been exaggerated: in the actual circuit, only signals from adjacent pixels converge. Furthermore, the detail of the averaging circuitry has not been included in this diagram.

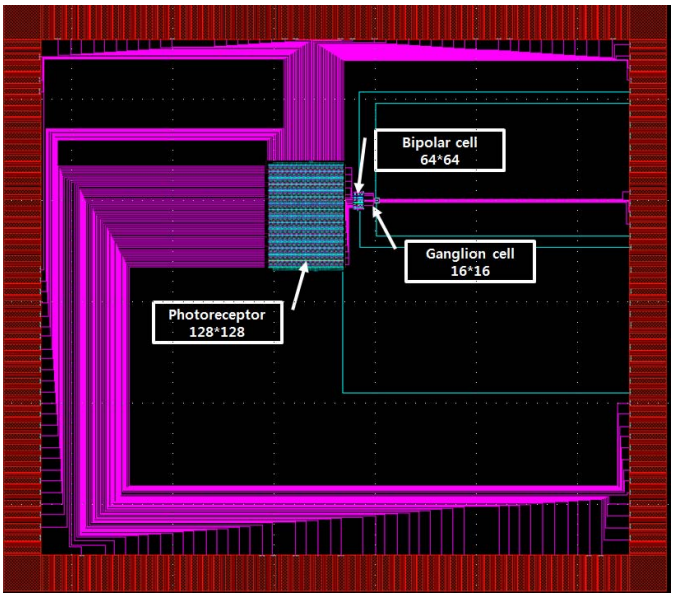

Fig. 14. Retinal network CMOS Chip: consisting of an array of 128 × 128 photoreceptor circuits, 64 × 64 bipolar cell circuits, and 16 × 16 ganglion cell circuits, fabricated using the SKHynix 180-nm process. The memristor layers are not shown in this layout structure, as they are die bonded to the CMOS chip on a separate layer.

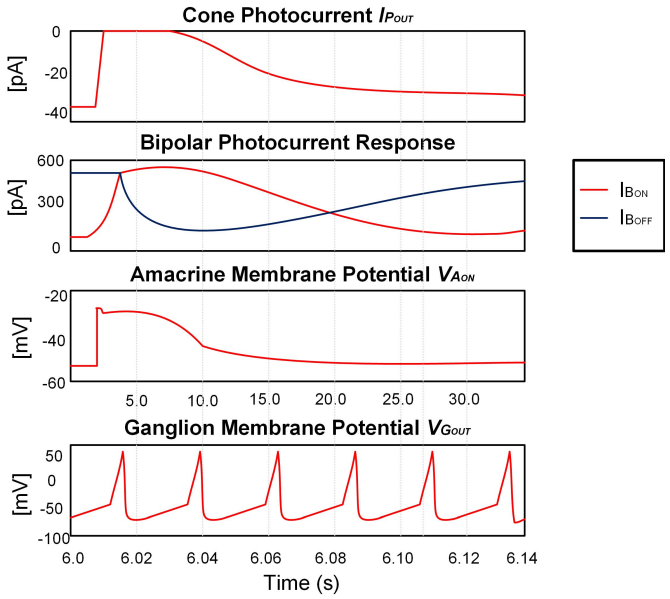

Fig. 15. Simulation result of a full retinal architecture network. The validity of each independent cellular circuit component has been confirmed in Section IV, and when the cells are connected as shown in Fig. 12 and extended outward into an array as in Fig. 14, each constituent component of the retina exhibits the appropriate voltage or current response, which further verifies the functionality of our architecture.

approximately fixed memristance when in either of two states, without having to decrease the ON–OFF memristance ratio. For the sake of completeness, in a circuit where the VTEAM model from [44] is used with parameters based on the Pt–Hf–Ti memristor from [50], with respect to Fig. 7, the curve between "1" and "2" is more gradual. This results in an averaged potential being displayed for a shorter duration of time before the signal spikes. Therefore, the system becomes more prone to errors if subject to noise, even though it is still adaptive into the architecture for the sake of image processing.

The input stimulus in the simulation was the emulation of a uniform light turning ON at 1 s for a duration of 0.02 s with a photocurrent injection of $I_{\mathrm{Ph}} = 600$ pA at the photodiode, which biologically corresponds to a light intensity of 100 rhodopsin/s and 50 000 photoisomerizations/cone/s. This was applied to the central photoreceptor circuit only, and all other photoreceptors were left without stimulation (for the initial setup). The results in Fig. 15 display the cone photocurrent response $I_{P_{\mathrm{OUT}}}$, the bipolar photocurrent

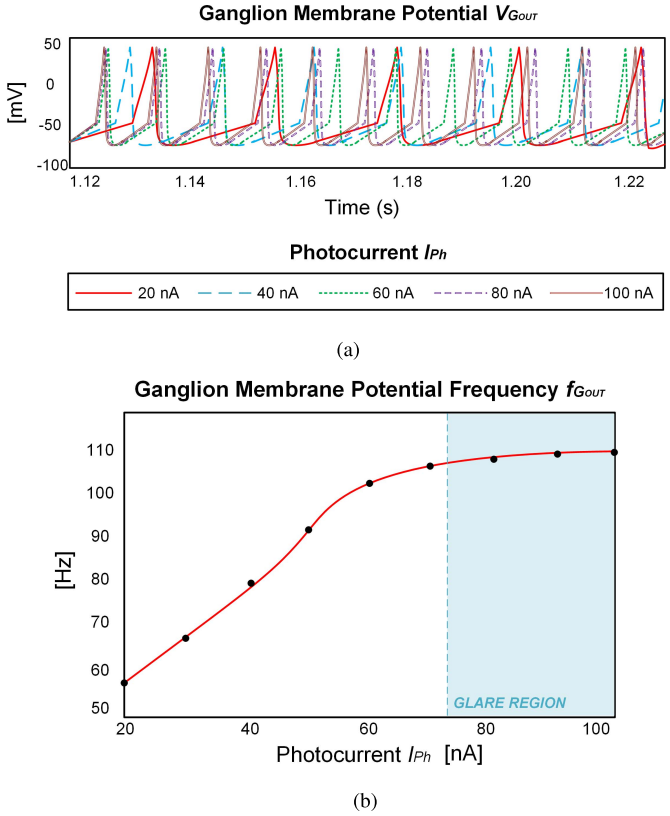

Fig. 16. Frequency analysis of the silicon retina output. The frequency of the various voltage responses $V_{G_{\mathrm{OUT}}}$ shown in Fig. 16(a) is approximately linear against photocurrent I_{Ph}, as shown in Fig. 16(b), until the system reaches saturation at approximately $I_{\mathrm{Ph}} \approx 75$ nA, beyond which is the glare region of the retina, where increase in light intensity can no longer be registered. The glare region can be shifted by using transistors of varying threshold values; however, the process used here provides an optimal tradeoff between retinal realism and power consumption. (a) Ganglion cell response to varying photocurrent input. (b) Ganglion cell frequency.

responses $I_{B_{\mathrm{ON}}}$ and $I_{B_{\mathrm{OFF}}}$, the amacrine membrane potential $V_{A_{\mathrm{ON}}}$, and most importantly, the ganglion membrane potential $V_{G_{\mathrm{OUT}}}$. These simulations match the shapes of experimentally verified cell behaviors as derived from computational models of the vertebrate retina [51]–[55].

Fig. 16(a) shows the ganglion membrane potential across varying values of input photocurrent I_{Ph}. The signal ceases to increase in frequency at input photocurrents of approximately 75 nA, which corresponds to the region where the retina ceases to be capable of differentiating increasing levels of light intensity (also known as the "glare region").

Fig. 16(b) presents the ganglion cell response $V_{G_{\mathrm{OUT}}}$ frequency $f_{G_{\mathrm{OUT}}}$ as a function of photocurrent at the photoreceptor cell I_{Ph}. Up until saturation, the relationship can be approximated by a linear model, which becomes significant in image reconstruction, which is the focus of the experimental results in Section VI-B.

This paper models cone terminals, horizontal cells, ON- and OFF-bipolar cells, amacrine cells, and ON- and OFF-ganglion cells, and for a single pathway consisting of one of each cell, it consumes a total of 7.8 μW of power. This includes dynamic, static, and leakage power during the activation

TABLE I
POWER CONSUMPTION OF A SINGLE CELL OUTPUT

Microprocessor	Retinal Chip [56]	Real Retina	This Work
2.2 mW	17 μW	16.2 nW	7.8 μW

TABLE II
POWER AND AREA PROJECTION

Process [57]	V_{DD} (V)	V_{Th} (V)	Active Power	Area
180 nm	1.8	0.4	1	1
45 nm	0.8	0.3	0.31	0.3
14 nm	0.5	0.25	0.09	0.24
10 nm	0.4	0.22	0.045	0.15

state of a single pathway. A comparison is made against other closely modeled circuits, as shown in Table I, where a typical microprocessor consumes 2.2 mW to simulate a single pathway from photoreceptor to ganglion cell, and a conventional retinal chip from [56] consumes 17 μW. For the full network pathway presented in this paper, a 128×128 array of photoreceptors consumes 8 μW, a 16×16 array of bipolar cells consumes 2 mW, and an 8×8 array of ganglion cells consumes 1 μW, and so the total power consumption for the layout can be approximated to 2 mW. The power consumption of the full retina containing 10^8 photoreceptors, 10^7 bipolar cells, and 10^6 ganglion cells can be estimated based on the measured data as 60 mW + 80 mW + 1 mW, which totals 141 mW.

In anticipation of power and area for advanced technologies and newer processes implementing the silicon retina presented in this paper, the data in Table II present a projection based on the 10-nm process devised by Samsung.

B. Image Processing Results

The simulation results match well with experimentally verified signal outputs, but a more meaningful result can be generated by interpreting the ganglion cell spike train as a proper image. As seen from Fig. 16, the range of meaningful frequencies the ganglion cell output produces is from $0 \rightarrow 105$ Hz. A Fourier transform is applied to the output of the chip to extract frequency data, and processed in MATLAB to linearly map the range of available frequencies from lowest to highest as 0 to 256 bits. Bit 256 is interpreted as white light (the highest possible frequency before saturation) and bit 0 as an absence of light (no output signal), linearly shifting gray-scale values in between.

Three examples are provided in Fig. 17. Each input image consists of a 128×128 array of pixels, and each pixel is either black or white, which corresponds to the 128×128 photoreceptor array. The maximum photocurrent value I_{Ph} before entering the glare region [as demonstrated in Fig. 16(b)] is approximately 75 nA, and so this photocurrent value is used to stimulate all white pixels. This photocurrent passes through the full network RRAM-CMOS neuromorphic vision chip to produce a spike train output from the 16×16 ganglion cell array. The spike train frequency value exists in the domain

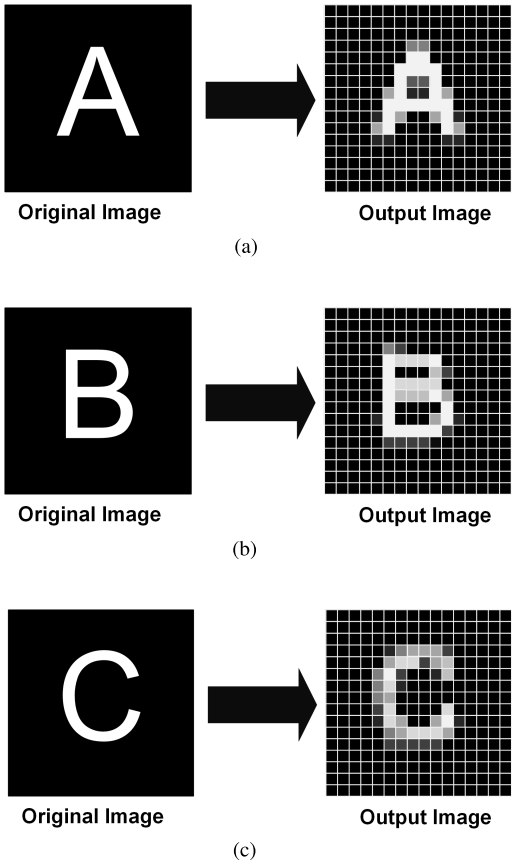

Fig. 17. Experimental results of a silicon retina network in full network array from 128 × 128 input image at the photoreceptor cell to the 16 × 16 array output at the ganglion cell. (a) Retinal network image processing of "A." (b) Retinal network image processing of "B." (c) Retinal network image processing of "C."

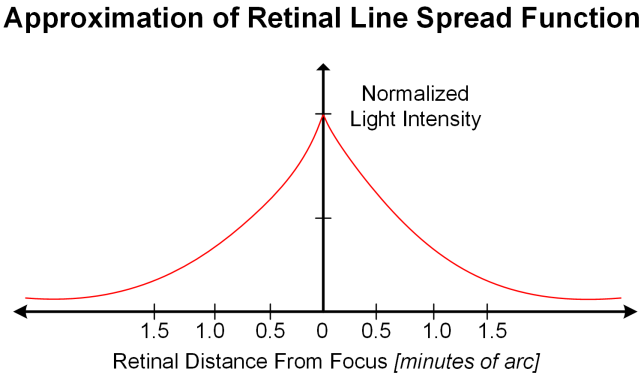

Fig. 18. Analytic approximation of the human line-spread function for an eye with a 3 mm diameter of the pupil adapted from [30]. The distance along the x-axis represents distance from the fovea across the back of the retina, and the line-spread function reflects the response of photoreceptors to a "perfect line" input as a function of light intensity.

[0, 105] [up to the maximum frequency value from Fig. 16(b)] and is mapped in MATLAB according to a linear scale to a bit value in the range [0, 256]. Each bit corresponds to a gray-scale value of monochromatic light and is presented as the ganglionic network response. In all cases, we see the

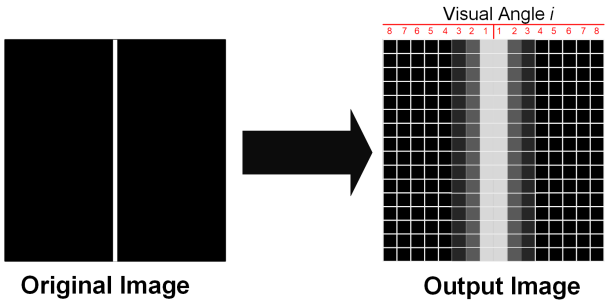

Fig. 19. Experimental results of a silicon network array from 128 × 128 input image at the photoreceptor cells to the 16 × 16 array at the ganglion cell output using a "fine line" input to determine the accuracy of our model by comparison to the human line-spread function. The center of the array is denoted as $i = 0'$ and each subsequent pixel column is 1 min of visual angle from the center.

practical advantage of our silicon retina chip of low-power image smoothing and conversion of a low-dynamic-range 2-bit black and white image into a 256-bit high-dynamic-range scene.

In fact, it is possible to test the accuracy of smoothing in our chip to that of the biological retina by comparing a single white line input to the line-spread function. The line spread of a system is the response to a 1-D line in a shift-invariant system. Naturally, as the pupil size increases, the width of the line-spread function also increases which indicates that the focus is worse for larger pupil sizes, and the amount of blurring increases. An analytic approximation of the human line-spread function for an eye with a 3-mm-diameter pupil is presented in [30], given in (8), graphed in Fig. 18, and is used as the benchmark for comparison of image processing against our chip

$$l_i = 0.47e^{-3.3i^2} + 0.53e^{-0.93|i|} \tag{8}$$

where l_i is the line-spread function, and the variable i refers to the position on the retina from the focal point specified in visual angle in minutes of arc, as experimentally validated by Westheimer. Applying this to a pixel array, the center of the array is denoted $i = 0$ and each subsequent pixel column is denoted as 1 min of visual angle from the center, demonstrated in Fig. 19 to capture a total of 16' arcminutes of visual angle in our experimental results.

Fig. 19 also shows the line-spread response of our silicon retina. Column $\pm i = 3$ generates a brightness of 24% white (i.e., 24% of the maximum frequency response). Substitution of $i = \pm 3$ into (8) yields 22.64%, which provides a very reasonable model of spatial smoothing within an error margin of 6%. This arises due to the lack of a perfect memristor behaving like a closed switch in the OFF state and, instead, dissipates power which ultimately has an effect on the frequency of the output.

VII. Conclusion

This paper proposes a low-power silicon RRAM-CMOS-based retinal network, which can generate four types of ganglion cell output signals, and was designed and verified with simulations and experimental results, mapped against

both biological data, and other neuromorphic vision processes. Memristors are used to provide functional averaging circuits to emulate spatial smoothing, and a low-dynamic-range integration APS to perceive a high-dynamic-range scene. Our efforts in replicating the significant complexity of retinal signal processing in a novel architecture involving cellular layers with interconnections across individual signal pathways are shown to be horizontally scalable and provide a basis for expansion to be implanted as part of a retinal prosthesis in the future, and ultimately pave the way for a new frontier in visual sensory systems.

REFERENCES

[1] D. Saha and A. Mukherjee, "Pervasive computing: A paradigm for the 21st century," *Computer*, vol. 36, no. 3, pp. 25–31, Mar. 2003.

[2] J. Gubbi, R. Buyya, S. Marusic, and M. Palaniswami, "Internet of Things (IoT): A vision, architectural elements, and future directions," *Future Generat. Comput. Syst.*, vol. 29, no. 7, pp. 1645–1660, 2013.

[3] C. A. Curcio, K. R. Sloan, R. E. Kalina, and A. E. Hendrickson, "Human photoreceptor topography," *J. Comparative Neurol.*, vol. 292, no. 4, pp. 497–523, 1990.

[4] C.-Y. Wu and H.-C. Jiang, "An improved BJT-based silicon retina with tunable image smoothing capability," *IEEE Trans. Very Large Scale Integr. (VLSI) Syst.*, vol. 7, no. 2, pp. 241–248, Jun. 1999.

[5] C. Mead, "Neuromorphic electronic systems," *Proc. IEEE*, vol. 78, no. 10, pp. 1629–1636, Oct. 1990.

[6] C. Mead and M. Ismail, Eds., *Analog VLSI Implementation of Neural Systems*, vol. 80. New York, NY, USA: Springer, 2012.

[7] J. Hutchinson, C. Koch, J. Luo, and C. Mead, "Computing motion using analog and binary resistive networks," *Computer*, vol. 21, no. 3, pp. 52–63, Mar. 1988.

[8] E. Zrenner *et al.*, "Subretinal electronic chips allow blind patients to read letters and combine them to words," *Proc. Roy. Soc. B, Biol. Sci.*, vol. 278, no. 1711, pp. 1489–1497, May 2011.

[9] J. G. Nicholls, A. R. Martin, B. G. Wallace, and P. A. Fuchs, *From Neuron to Brain*, vol. 271. Sunderland, MA, USA: Sinauer Associates, 2001.

[10] R. H. Masland, "The fundamental plan of the retina," *Nature Neurosci.*, vol. 4, no. 9, pp. 877–886, 2001.

[11] D. A. Baylor, A. L. Hodgkin, and T. D. Lamb, "The electrical response of turtle cones to flashes and steps of light," *J. Physiol.*, vol. 242, no. 3, pp. 685–727, 1974.

[12] R. D. Hamer and C. W. Tyler, "Phototransduction: Modeling the primate cone flash response," *Vis. Neurosci.*, vol. 12, no. 6, pp. 1063–1082, 1995.

[13] V. Kefalov, Y. Fu, N. Marsh-Armstrong, and K.-W. Yau, "Role of visual pigment properties in rod and cone phototransduction," *Nature*, vol. 425, no. 6957, pp. 526–531, Oct. 2003.

[14] J. I. Korenbrot, "Speed, adaptation, and stability of the response to light in cone photoreceptors: The functional role of Ca-dependent modulation of ligand sensitivity in cGMP-gated ion channels," *J. General Physiol.*, vol. 139, no. 1, pp. 31–56, 2012.

[15] M. Tessier-Lavigne and D. Attwell, "The effect of photoreceptor coupling and synapse nonlinearity on signal: Noise ratio in early visual processing," *Proc. Roy. Soc. London B, Biol. Sci.*, vol. 234, no. 1275, pp. 171–197, 1988.

[16] K. Cho *et al.*, "Signal flow platform for mapping and simulation of vertebrate retina for sensor systems," *IEEE Sensors J.*, vol. 16, no. 15, pp. 5856–5866, Aug. 2016.

[17] J. K. Eshraghian *et al.*, "Modelling and analysis of signal flow platform implementation into retinal cell pathway," in *Proc. IEEE Asia Pacific Conf. Circuits Syst. (APCCAS)*, Oct. 2016, pp. 491–494.

[18] J. Barnes, *Essential Biological Psychology*. Newbury Park, CA, USA: Sage, 2013.

[19] J. Hasler and B. Marr, "Finding a roadmap to achieve large neuromorphic hardware systems," *Frontiers Neurosci.*, vol. 7, p. 118, Sep. 2013.

[20] L. Chua, "Memristor—The missing circuit element," *IEEE Trans. Circuit Theory*, vol. 18, no. 5, pp. 507–519, Sep. 1971.

[21] D. B. Strukov, G. S. Snider, D. R. Stewart, and R. S. Williams, "The missing memristor found," *Nature*, vol. 453, no. 7191, p. 80, 2008.

[22] S. H. Jo, T. Chang, I. Ebong, B. B. Bhadviya, P. Mazumder, and W. Lu, "Nanoscale memristor device as synapse in neuromorphic systems," *Nano Lett.*, vol. 10, no. 4, pp. 1297–1301, 2010.

[23] A. P. James, D. S. Kumar, and A. Ajayan, "Threshold logic computing: Memristive-CMOS circuits for fast fourier transform and vedic multiplication," *IEEE Trans. Very Large Scale Integr. (VLSI) Syst.*, vol. 23, no. 11, pp. 2690–2694, Nov. 2015.

[24] C. Zamarreño-Ramos, L. A. Camuñas-Mesa, J. A. Pérez-Carrasco, T. Masquelier, T. Serrano-Gotarredona, and B. Linares-Barranco, "On spike-timing-dependent-plasticity, memristive devices, and building a self-learning visual cortex," *Frontiers Neurosci.*, vol. 5, p. 26, Mar. 2011.

[25] T. Serrano-Gotarredona, T. Masquelier, T. Prodromakis, G. Indiveri, and B. Linares-Barranco, "STDP and STDP variations with memristors for spiking neuromorphic learning systems," *Frontires Neurosci.*, vol. 7, p. 2, Feb. 2013.

[26] A. Gelencsér, T. Prodromakis, C. Toumazou, and T. Roska, "Biomimetic model of the outer plexiform layer by incorporating memristive devices," *Phys. Rev. E, Stat. Phys. Plasmas Fluids Relat. Interdiscip. Top.*, vol. 85, no. 4, p. 041918, Apr. 2012.

[27] S. N. Mozaffari, S. Tragoudas, and T. Haniotakis, "More efficient testing of metal-oxide memristor–based memory," *IEEE Trans. Comput.-Aided Des. Integr. Circuits Syst.*, vol. 36, no. 6, pp. 1018–1029, Jun. 2017.

[28] A. L. Hodgkin and A. F. Huxley, "A quantitative description of membrane current and its application to conduction and excitation in nerve," *J. Physiol.*, vol. 117, no. 4, pp. 500–544, 1952.

[29] R. Publio, R. F. Oliveira, and A. C. Roque, "A computational study on the role of gap junctions and rod I_h conductance in the enhancement of the dynamic range of the retina," *PLoS ONE*, vol. 4, no. 9, p. e6970, 2009.

[30] B. A. Wandell, *Foundations of Vision*. Sunderland, MA, USA: Sinauer Associates, 1995.

[31] J. E. Dowling, *The Retina: An Approachable Part of the Brain*. Cambridge, MA, USA: Harvard Univ. Press, 1987.

[32] D. Regan, *Human Perception of Objects*. Sunderland, MA, USA: Sinauer Associates, 2000, pp. 295–342.

[33] F. H. Eeckman, M. E. Colvin, and T. S. Axelrod, "A retina-like model for motion detection," in *Proc. Int. Joint Conf. Neural Netw.*, vol. 2. 1989, pp. 247–249.

[34] S. L. Jackman, N. Babai, J. J. Chambers, W. B. Thoreson, and R. H. Kramer, "A positive feedback synapse from retinal horizontal cells to cone photoreceptors," *PLoS Biol.*, vol. 9, no. 5, p. e1001057, 2011.

[35] J.-W. Lee, S.-P. Chae, M.-N. Kim, S.-Y. Kim, and J.-H. Cho, "A moving detectable retina model considering the mechanism of an amacrine cell for vision," in *Proc. IEEE Int. Symp. Ind. Electron. (ISIE)*, vol. 1. Jun. 2001, pp. 106–109.

[36] J. F. Fohlmeister, P. A. Coleman, and R. F. Miller, "Modeling the repetitive firing of retinal ganglion cells," *Brain Res.*, vol. 510, no. 2, pp. 343–345, Mar. 1990.

[37] L. O. Chua, "If it's pinched it's a memristor," *Semicond. Sci. Technol.*, vol. 29, no. 10, p. 104001, 2014.

[38] D. Yu, H. H.-C. Iu, Y. Liang, T. Fernando, and L. O. Chua, "Dynamic behavior of coupled memristor circuits," *IEEE Trans. Circuits Syst. I, Reg. Papers*, vol. 62, no. 6, pp. 1607–1616, Jun. 2015.

[39] J. K. Eshraghian, H. H. C. Iu, T. Fernando, D. Yu, and Z. Li, "Modelling and characterization of dynamic behavior of coupled memristor circuits," in *Proc. IEEE Int. Symp. Circuits Syst. (ISCAS)*, May 2016, pp. 690–693.

[40] D. Holcman and J. I. Korenbrot, "The limit of photoreceptor sensitivity: Molecular mechanisms of dark noise in retinal cones," *J. General Physiol.*, vol. 125, no. 6, pp. 641–660, 2005.

[41] Y. N. Joglekar and S. J. Wolf, "The elusive memristor: Properties of basic electrical circuits," *Eur. J. Phys.*, vol. 30, no. 4, p. 661, 2009.

[42] S. Shin, L. Zheng, G. Weickhardt, S. Cho, and S.-M. Kang, "Compact circuit model and hardware emulation for floating memristor devices," *IEEE Circuits Syst. Mag.*, vol. 13, no. 2, pp. 42–55, 2nd Quart., 2013.

[43] L. Zheng, S. Shin, and S. M. S. Kang, "Unified modeling for memristive devices based on charge-flux constitutive relationships," in *Proc. IEEE Int. Symp. Circuits Syst. (ISCAS)*, May 2013, pp. 213–216.

[44] S. Kvatinsky, M. Ramadan, E. G. Friedman, and A. Kolodny, "VTEAM: A general model for voltage-controlled memristors," *IEEE Trans. Circuits Syst. II, Exp. Briefs*, vol. 62, no. 8, pp. 786–790, Aug. 2015.

[45] S. Ha, "An ultra low power silicon retina with spatial and temporal filtering," Univ. California, San Diego, La Jolla, CA, USA, Tech. Rep., 2010.

[46] T. Euler and R. H. Masland, "Light-evoked responses of bipolar cells in a mammalian retina," *J. Neurophysiol.*, vol. 83, no. 4, pp. 1817–1829, 2000.

[47] S. W. Kuffler, "Discharge patterns and functional organization of mammalian retina," *J. Neurophysiol.*, vol. 16, no. 1, pp. 37–68, Jan. 1953.

[48] Z. Biolek, D. Biolek, and V. Biolkova, "SPICE model of memristor with nonlinear dopant drift," *Radioengineering*, vol. 18, no. 2, pp. 210–214, 2009.
[49] S. Shin, K. Kim, and S.-M. Kang, "Compact models for memristors based on charge-flux constitutive relationships," *IEEE Trans. Comput.-Aided Des. Integr. Circuits Syst.*, vol. 29, no. 4, pp. 590–598, Apr. 2010.
[50] E. Yalon *et al.*, "Resistive switching in HfO_2 probed by a metal–insulator–semiconductor bipolar transistor," *IEEE Electron Device Lett.*, vol. 33, no. 1, pp. 11–13, Jan. 2012.
[51] Y. Kamiyama, S. M. Wu, and S. Usui, "Simulation analysis of bandpass filtering properties of a rod photoreceptor network," *Vis. Res.*, vol. 49, no. 9, pp. 970–978, May 2009.
[52] Y. Kamiyama, T. O'Sura, and S. Usui, "Ionic current model of the vertebrate rod photoreceptor," *Vis. Res.*, vol. 36, no. 24, pp. 4059–4068, Dec. 1996.
[53] S. Usui, A. Ishihaiza, Y. Kamiyama, and H. Ishii, "Ionic current model of bipolar cells in the lower vertebrate retina," *Vis. Res.*, vol. 36, no. 24, pp. 4069–4076, Dec. 1996.
[54] J. K. Eshraghian *et al.*, "Formulation and implementation of nonlinear integral equations to model neural dynamics within the vertebrate retina," *Int. J. Neural Syst.*, Apr. 2018, doi: https://doi.org/10.1142/S0129065718500041
[55] *Mathematical Model of Retinal Cells*. Accessed: Feb. 28, 2018. [Online]. Available: http://ccns.cbnu.ac.kr/paper/1605/appendix.pdf
[56] K. A. Zaghloul and K. Boahen, "A silicon retina that reproduces signals in the optic nerve," *J. Neural Eng.*, vol. 3, no. 4, pp. 257–267, 2006.
[57] H.-J. Cho *et al.*, "Si FinFET based 10nm technology with multi Vt gate stack for low power and high performance applications," in *Proc. IEEE Symp. VLSI Technol.*, Jun. 2016, pp. 1–2.

Jason Kamran Eshraghian, Jr. (S'15) received the B.Eng. degree in electrical and electronic engineering and the LL.B. degree from The University of Western Australia, Crawley, WA, Australia, in 2017, where he is currently working toward the Ph.D. degree.

From 2015 to 2016, he was a Visiting Student at Chungbuk National University, Cheongju, South Korea. His current research interests include memristive systems, computational neuroscience, and neural networks.

Dr. Eshraghian, Jr. was a recipient of the Best Presentation Award for his undergraduate thesis at The University of Western Australia.

Kyoungrok Cho (S'89–M'92) received the B.S. degree in electronics engineering from Kyoungpook National University, Daegu, South Korea, in 1977, and the M.S. and Ph.D. degrees in electrical engineering from The University of Tokyo, Tokyo, Japan, in 1989 and 1992, respectively.

From 1979 to 1986, he was with the TV Research Center, LG Electronics, Seoul, South Korea. In 1999 and 2006, he was with Oregon State University, Corvallis, OR, USA, as a Visiting Scholar. He is currently a Professor at the College of Electrical and Computer Engineering, Chungbuk National University, Cheongju, South Korea, where he is also the Director of the IC Design Education Center. His current research interests include high-speed and low-power circuit designs, SoC platform design for communication systems, and prospective CMOS image sensors, memristor-based circuits, and the design of multilayer system-on-systems technology.

Dr. Cho is a member of the Institute of Electronics Engineers of Korea (IEEK). He was a recipient of the IEEK Award in 2004.

Ciyan Zheng (S'17) received the B.S. degree in electrical engineering from the China University of Mining and Technology, Xuzhou, China, in 2015. She is currently working toward the Ph.D. degree at The University of Western Australia, Crawley, WA, Australia.

Her current research interests include nonlinear circuit dynamics, memristive systems, and microgrids.

Minho Nam (S'16) received the B.S. and M.S. degrees in information and communication engineering from Chungbuk National University, Cheongju, South Korea, in 2013 and 2015, respectively, where he is currently working toward the Ph.D. degree at the Department of Information and Communication Engineering.

His current research interests include high-speed and low-power circuit designs, system-on-chip designs, and CMOS image sensors.

Herbert Ho-Ching Iu (S'98–M'00–SM'06) received the B.Eng. degree (honors) in electrical and electronic engineering from The University of Hong Kong, Hong Kong, in 1997, and the Ph.D. degree from The Hong Kong Polytechnic University, Hong Kong, in 2000.

In 2002, he joined the School of Electrical, Electronic and Computer Engineering, The University of Western Australia, Crawley, WA, Australia, as a Lecturer, where he is currently a Professor. He has coedited the book *Control of Chaos in Nonlinear Circuits and Systems* (Singapore: World Scientific, 2009) and coauthored the book *Development of Memristor Based Circuits* (Singapore: World Scientific, 2013). His current research interests include power electronics, renewable energy, nonlinear dynamics, complex networks, and memristive systems. He has published over 100 papers in these areas.

Dr. Iu received two IET Premium Awards in 2012 and 2014, the Vice-Chancellor's Mid-Career Research Award in 2014, and the IEEE PES Chapter Outstanding Engineer Award in 2015. He currently serves as an Associate Editor for the IEEE TRANSACTIONS ON CIRCUITS AND SYSTEMS II: EXPRESS BRIEFS, the IEEE TRANSACTIONS ON POWER ELECTRONICS, and IEEE ACCESS, an Editor for the IEEE TRANSACTIONS ON SMART GRID, and an Editorial Board Member for the IEEE JOURNAL OF EMERGING AND SELECTED TOPICS IN CIRCUITS AND SYSTEMS and the *International Journal of Circuit Theory and Applications*.

Wen Lei received the B.S. and M.S. degrees in material science and engineering from the China University of Geoscience, Wuhan, China, in 2000 and 2003, respectively, and the Ph.D. degree in semiconductor materials and devices from the Institute of Semiconductors, Chinese Academy of Sciences, Beijing, China, in 2006.

From 2006 to 2007, he was a Postdoctoral Researcher at the University of Duisburg-Essen, Duisburg, Germany. From 2007 to 2012, he was an Australian Postdoctoral Fellow at the Australian Research Council (ARC) and a Research Fellow at The Australian National University, Canberra, ACT, Australia. In 2012, he joined the School of Electrical, Electronic and Computer Engineering, The University of Western Australia, Crawley, WA, Australia, as an Associate Professor, where he is currently a Professor. His current research interests include semiconductor thin film and nanostructure materials and their applications in microelectronic and optoelectronic devices.

Dr. Lei was a recipient of the prestigious ARC Future Fellowship in 2013.

Kamran Eshraghian received the B.Tech., M.Eng.Sc., and Ph.D. degrees from The University of Adelaide, Adelaide, SA, Australia, in 1969, 1977, and 1980, respectively, and the Dr.-Ing. degree from the University of Ulm, Ulm, Germany, in 2004, for his research into integration of nanoelectronics with that of the light wave technology.

He is best known in the international arena as being one of the fathers of CMOS VLSI having influenced two generations of researchers in both academia and industry. In 1979, he joined the Department of Electrical and Electronic Engineering, The University of Adelaide, after spending ten years with Philips Research in Australia and Europe. In 1994, he was invited to take up the Foundation Chair of Computer Electronic and Communications Engineering, The University of Western Australia, Crawley, WA, Australia, and became the Head of the School of Engineering and Mathematics, and subsequently became a Distinguished Professor and the Director with the Electron Science Research Institute. In 2004, he became the Founder/President of Elabs, Perth, WA, Australia, as part of his vision for the integration of nanoelectronics with those of bio- and photo-based technologies, thus creating a new domain for system on system integration. In 2007, he was the holder of the inaugural Ferrero Family Chair of Electrical Engineering and a Visiting Professor of Engineering with the University of California at Merced, Merced, CA, USA. In 2009, he joined Chungbuk National University, Cheongju, South Korea, as a Distinguished Professor of the World Class University Program. He is currently the President of iDataMap Corporation, Eastwood, SA, Australia, and serves as the Executive Chairman of the Board of Directors. He has founded six high technology companies, providing intimate links between university research and industry. He has coauthored six books and has lectured widely in very large-scale integrated and multitechnology systems. His current research interests include eHealth and healthcare with a particular emphasis on computational neuroscience.

Dr. Eshraghian is a Fellow and Life Member of the Institution of Engineers, Australia.